Atmospheric Environment 43 (2009) 5731–5742

Contents lists available at ScienceDirect

Atmospheric Environment

journal homepage: www.elsevier.com/locate/atmosenv

An observational study of the HONO–NO_2 coupling at an urban site in Guangzhou City, South China

Min Qin [a,*], Pinhua Xie [a], Hang Su [b], Jianwei Gu [b], Fumin Peng [a], Suwen Li [a], Limin Zeng [b], Jianguo Liu [a], Wenqing Liu [a], Yuanhang Zhang [b]

[a] Key Lab. of Environmental Optics & Technology, Anhui Institute of Optics and Fine Mechanics, Chinese Academy of Sciences, Hefei 230031, China
[b] State Joint Key Laboratory of Environmental Simulation and Pollution Control, College of Environmental Sciences and Engineering, Peking University, Beijing 100871, China

ARTICLE INFO

Article history:
Received 4 November 2008
Received in revised form
10 August 2009
Accepted 11 August 2009

Keywords:
Atmospheric chemistry
Air pollution
Heterogeneous conversion
Nitrous acid
DOAS

ABSTRACT

The temporal behavior of HONO and NO_2 was investigated at an urban site in Guangzhou city, China, by means of a DOAS system during the Pearl River Delta 2006 intensive campaign from 10 to 24 July 2006. Within the whole measurement period, unexpected high HONO mixing ratios up to 2 ppb were observed even during the day. A nocturnal maximum concentration of about 8.43 ± 0.4 ppb was detected on the night of 24 July 2006. Combining the data simultaneously observed by different instruments, the coupling of HONO–NO_2 and the possible formation sources of HONO are discussed. During the measurement period, concentration ratios of HONO to NO_2 ranged from (0.03 ± 0.1) to (0.37 ± 0.09), which is significantly higher than previously reported values (0.01–0.1). Surprisingly, in most cases a strong daytime correlation between HONO and NO_2 was found, contrary to previous observations in China. Aerosol was found to have a minor impact on HONO formation during the whole measurement period. Using a pseudo steady state approach for interpreting the nocturnal conversion of NO_2 to HONO suggests a non-negligible role of the relative humidity for the heterogeneous HONO formation from NO_2.

1. Introduction

Nitrous acid (HONO) plays an important role in atmospheric chemistry because of its photolysis

$$HONO + h\upsilon(300\ nm < \lambda < 405\ nm) \rightarrow NO + OH, \quad (R1)$$

thus providing an efficient source of the hydroxyl (OH) radical which, due to its high reactivity, is a key intermediate for all photochemical atmospheric processes, particularly the formation of photochemical smog (Pitts et al., 1984; Alicke et al., 2002). Recently, unexpected high daytime HONO concentrations of up to several hundred ppt were observed in a number of field studies not only in the urban polluted but also in rural areas in Europe (Veitel et al., 2002; Kleffmann et al., 2005, 2006; Acker et al., 2006a; Acker et al., 2006b). By simultaneously measuring the concentrations of OH and NO, as well as the photolysis rate J of HONO, J(HONO), Kleffmann et al. (2005) and Acker et al. (2006b) experimentally verified that a strong unknown daytime source of HONO exists and, consequently, the contribution of HONO to the OH budget needs to be reconsidered. Kleffmann (2007) suggested that HONO is mainly formed by heterogeneous processes, i.e. surface reactions of NO_2. But to date, the exact mechanism of HONO formation is not clear, especially not for its daytime source. Also, the role which aerosols play in the formation of HONO is still under discussion (Broske et al., 2003; Gustafsson et al., 2006; Stemmler et al., 2007). In the following, we sum up the currently established formation pathways of HONO.

1.1. Direct emission

HONO can be directly emitted into the troposphere via combustion processes, e.g. vehicle exhaust, or biomass burning. However, traffic tunnel studies have shown that on average only 0.3–0.8% of the total traffic induced NO_x ($NO + NO_2$) can be attributed to direct HONO emissions (Kirchstetter et al., 1996; Kurtenbach et al., 2001). In other words, direct traffic emission can account for actual atmospheric HONO concentrations only in heavily polluted areas with high traffic volume.

* Corresponding author. Tel.: +86 551 5593348; fax: +86 551 5591530.
E-mail address: mqin@aiofm.ac.cn (M. Qin).

1352-2310/$ – see front matter © 2009 Elsevier Ltd. All rights reserved.
doi:10.1016/j.atmosenv.2009.08.017

1.2. Homogeneous reactions

The most important homogeneous reaction forming HONO is the reverse process of reaction (R1) (Stuhl and Niki, 1972; Pagsberg et al., 1997; Nguyen et al., 1998; Alicke et al., 2002):

$$NO + OH + M \rightarrow HONO + M \quad (R2)$$

This reaction is considered to be only important during the daytime period when OH and NO concentrations are high; it cannot explain high levels of HONO during the night. Recently, based on laboratory studies, the gas reactions involving the gas phase photolysis of different ortho-nitrophenols and methyl-2-nitrophenols were proposed as sources of HONO (Bejan et al., 2006, 2007), but their significance still needs to be verified in field observations.

Another recent finding reported by Li et al. (2008) suggests that excited NO_2 can react with water molecules to form HONO and OH:

$$NO_2 + h\upsilon(\lambda > 420\ nm) \rightarrow NO_2^* \quad (R3)$$

$$NO_2^* + M \rightarrow NO_2 + M(\text{where M is } N_2, O_2, \text{or } H_2O) \quad (R4)$$

$$NO_2^* + H_2O \rightarrow OH + HONO \quad (R5)$$

Although the rate constant of (R5) needs to be further investigated, first results illustrate the significance of this pathway for special conditions, e.g. high solar zenith angles in a polluted urban environment.

1.3. Heterogeneous reactions

The following stoichiometries describe the heterogeneous conversion of NO_2 adsorbed on humid surfaces or particles (Svensson et al., 1987; Finlayson-Pitts et al., 2003; Ammann et al., 1998; Kleffmann et al., 1998; Gutzwiller et al., 2002):

$$2NO_2 + H_2O \rightarrow HONO + HNO_3 \quad (R6)$$

$$NO_2 + HC_{red} \rightarrow HONO + HC_{ox} \quad (R7)$$

Two other heterogeneous reactions have been suspected as daytime sources of HONO: the photolysis of absorbed nitrate (NO_3^-) or nitric acid (HNO_3) (Zhou et al., 2001, 2002, 2003; Ramazan et al., 2004)

$$HNO_3/NO_3^- + h\upsilon \rightarrow HONO/NO_2^- + O \quad (R8)$$

and the photosensitized reduction of NO_2 on organic surfaces (e.g. aromatic hydrocarbons or humid acids) (George et al., 2005; Stemmler et al., 2006)

$$A_{red} + NO_2 \rightarrow A'' + HONO(A_{red} = \text{a reduced photosensitiser}) \quad (R9)$$

In general, NO_2 is regarded as an important precursor of HONO (One possible pathway is given by the daytime formation of HNO_3 from the reaction of NO_2 with OH and its subsequent photolysis (R8)). In field studies HONO has always shown positive correlation with NO_2 (or $NO_2 \cdot NO$) (e.g. Lammel and Cape, 1996; Andres-Hernandez et al., 1996; Alicke et al., 2003; Acker et al., 2004; Fisseha et al., 2006). Considering the ratio of HONO to NO_2 reduces the impact of transport processes and makes it a useful parameter for the discussion of HONO sources (Acker et al., 2006a; Reisinger, 2000; Andres-Hernandez et al., 1996).

Despite its importance for the atmospheric chemistry, only few studies have been devoted to HONO field measurements in China, and there is still a considerable lack of information on typical HONO concentrations in both urban and rural environments. However, with high primary pollutants and aerosol concentrations, the photochemical system in China can be expected to be sometimes quite different from the one observed in developed countries. Recently, high levels of HONO have been reported in several field studies conducted in some of China's largest cities (e.g. Beijing, Shanghai and Guangzhou) (Qin et al., 2006; Hao et al., 2006; Hu et al., 2002). Guangzhou lies in the Pearl River Delta (PRD), also including Shenzhen and Hong Kong – a region of rapidly growing export orientated manufacturing industry (Guangdong Statistical Yearbook, 2006), leading to serious air pollution problems. Early-morning HONO concentrations of up to ~12 ppb were observed in Guangzhou in June 2000 (Hu et al., 2002). Enhanced average values of HONO in Guangzhou were also found in a more recent diurnal analysis, with mean noon values up to 2 ppb (Zhang et al., 2008). But high daytime HONO levels occurred even at the rural site of Xinken, in the South of the PRD (Su et al., 2008a,b). Studying the impact of enhanced concentrations occurring between 0900 LT (local time) and 1500 LT on O_3 and radical formation, the authors model an OH formation rate up to three times faster than that from O_3 photolysis.

Currently, mainly three detection methods are employed in HONO field measurements: Differential Optical Absorption Spectroscopy (DOAS), wet chemical methods based on denuder techniques and the long path absorption photometer (LOPAP) technique which combines wet chemical sampling and photometric detection. The recent PRD measurements were mainly performed using the denuder method, demonstrated to suffer from chemical interferences (Su et al., 2008a; Gu et al., 2009). The present work is based on the DOAS technique and, to our knowledge, the first application of a DOAS system in the subtropics of China. The trace gases HONO, NO_2, SO_2, O_3 and HCHO were measured by DOAS, while other trace gases and meteorological parameters were monitored simultaneously from 10–24 July 2006 to investigate ratios and correlations of HONO to NO_2 during this period. The impacts of traffic emissions, aerosol and RH on HONO formation are also discussed.

2. Experimental section

2.1. Measurement site

The DOAS measurements were part of the PRIDE-PRD2006 intensive campaign (ACPD – Special Issue, PRIDE-PRD2006 http://www.atmos-chem-phys-discuss.net/special_issue101.html), covering the period from 3 to 24 July in Guangzhou city. The DOAS sending and receiving telescope was set up on the 16th floor (about 55 m above ground) of the building of the Guangdong Provincial Environmental Protection Monitoring Center (23°8′4.10N, 113°15′52.50E) (see Fig. 1). The light path was folded by a retroreflector array which was mounted at a distance of about 425 m on top of the downtown Jinhe buildings at a height of about 70 m. The light path crossed gaps between several high buildings and a residential area with flat buildings surrounded by heavy traffic lines and several parks in the North-West of the measurement site.

2.2. Measurement techniques

2.2.1. DOAS instrument and data evaluation

The set up of the DOAS instrument employed in the PRD campaign has been described in detail elsewhere (Qin et al., 2006) so that we confine ourselves here to a brief summary of the DOAS retrieval. For data quality assurance, the calibration of the DOAS system including measurements of the spectra of a mercury and xenon lamp was conducted every day at noon. The wavelength coverage of 287.9–370.8 nm allows monitoring O_3, SO_2, HCHO, NO_2

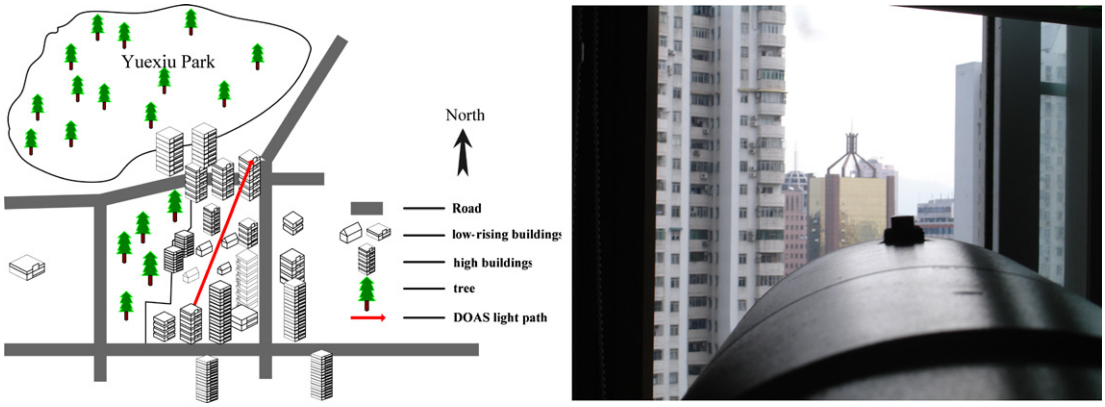

Fig. 1. Sketch of the monitoring site. The light path of the DOAS system has a total length of 850 m crossing a flat residential area pointing to the North-East. The average vertical distance between light path and the low-rising building surfaces is about 40 m, and the horizontal distance between light path and nearby high buildings varies from several meters to tens of meters.

and HONO. Each coadded spectrum consists of approximately 30 spectra recorded with a spectral resolution of 0.25 nm (FWHM) in an interval of 83 nm. The time resolution of the measurements varied between 2 and 5 min, depending on visibility. In the remainder of this work, we only focus on the retrieval of HONO and NO_2. The spectral range used for their spectral analysis was 336–370 nm where HONO exhibits three distinct absorption peaks (342, 354 and 368.1 nm) (Stutz et al., 2000) allowing a reliable detection. Subsequent steps of the standard DOAS procedure (e.g. Stutz and Platt, 1996) consist in high pass filtering, taking the logarithm, smoothing and finally applying a combined linear–nonlinear least squares fit to obtain the concentrations of HONO and NO_2 as fit coefficients of the calibrated reference spectra.

Fig. 2 shows an example evaluation of an atmospheric spectrum (Fig. 2A, thin line) taken during daytime. The thick lines in Fig. 2A–C represent the reference spectra of NO_2, HCHO and HONO respectively. The remaining residual structure after subtracting the reference spectra is shown in the bottom panel (Fig. 2D). The residual structures amount to no more than 8.4×10^{-4} from peak to peak.

Table 1 lists wavelength intervals and literature absorption cross section used in this study, as well as observed mean concentrations and detection limits of all detected species for the period from 10 to 24 July. Mean detection limits were calculated according to Stutz and Platt (1996).

2.2.2. Other instruments

Apart from detection by DOAS, HONO was also measured by an in-situ gas and aerosol collector-GAC system (based on the wet denuder sampling method) combined with ion chromatography, which was developed by Peking University (PKU) (Gu et al., 2009). The GAC can measure both aerosol components (e.g. NO_2^-, NO_3^-) and related gas species (e.g. HONO, HNO_3) simultaneously, the former being collected in the first 15 min of the detection time, the latter in its remaining 15 min. The system had a 15-min sampling period within a 30-min cycle. The detection limits of Cl^-, NO_2^-, NO_3^- and

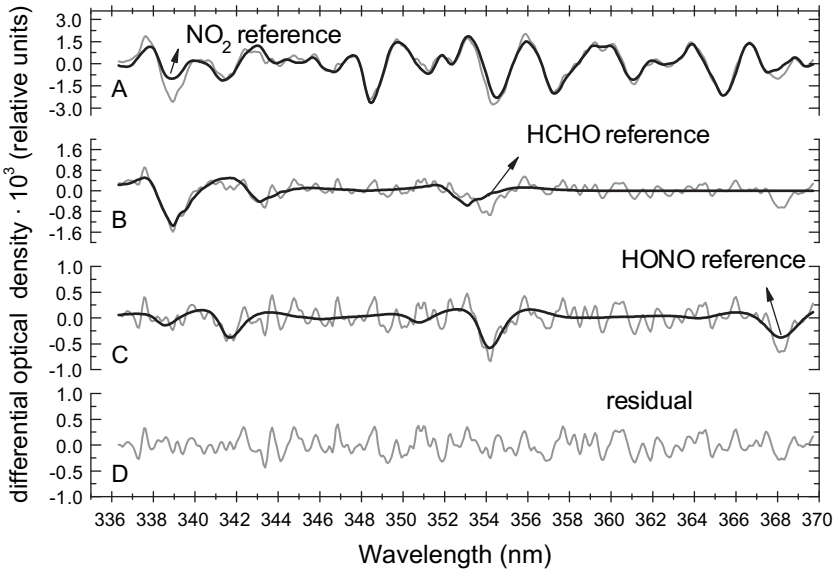

Fig. 2. Evaluation of a single spectrum recorded between 336 nm and 370 nm for detection of HONO and NO_2 on 13 July 2006 at 1155 LT. A shows the atmospheric spectrum (thin line) and the reference spectrum of the main absorber NO_2 (thick line). The spectral structure of HONO (1.05 ± 0.071 ppb, see panel C) can be clearly identified after removing the very strong absorption structure of NO_2 (15.6 ± 0.15 ppb) and the smaller structure of HCHO (17.8 ± 0.62 ppb, see panel B). D shows the residual spectrum of about 8×10^{-4} (peak-to-peak value) after fitting all trace gases.

Table 1
Overview of measured species and observed mixing ratios for 10–24 July 2006. Here, the relative error is the uncertainty of the absorption cross section given in the respective references.

Species	Wavelength interval, nm	Absorption cross section σ_a	Rel. σ_a-error	Mean mixing ratio, ppb	Mean detection limit,[a] ppb
NO_2	336–370	(Voigt et al., 2002)	±3.5%	30.3	0.87
HONO	336–370	(Stutz et al., 2000)	±5%	2.8	0.41
HCHO	290–335	(Meller and Moortgat, 2000)	±5%	8.1	1.65
O_3	290–335	(Voigt et al., 2001)	±3–7%	22.8	3.5
SO_2	290–335	(Vandaele et al., 1994)	±2.4%	39.1	0.13

[a] Light path length 850 m.

SO_4^{2-} are about 0.243, 0.358, 0.443 and 0.328 μg m^{-3}, respectively. For gas HONO, the detection limit is about 65 ppt with an uncertainty of about 10%. The species O_3, NO/NO_2, SO_2 and CO were measured by means of the commercial instruments EC 9810B, 9841B, 9850B, 9830B from the company Ecotech with detection limits about 0.5, 0.4, 0.5 and 4 ppb, respectively. Calibration was performed every day at midnight. PM10 was measured using the commercial R&P TEMO ambient particulate monitor. The aerosol size distributions obtained by TDMPS (TSI3080) and APS (Aerodynamic Particle Sizer, TSI 3321) instruments with a time resolution of both 5 min were used to calculate the surface area-to-volume ratio $S/V_{aerosol}$ of PM10, as reported by Cheng et al. (2006). All the above instruments were operated by the group of PKU.

The commercial instruments and the GAC were located on the 17th floor of the same building as the DOAS system. Any sample inlets consisted of Teflon tubes attached to the roof of the building. A weather station run by Sun Yet-Sen University automatically collected 10 min averages of solar radiation (SR), rainfall, pressure, relative humidity (RH), air temperature and wind speed and direction.

3. Result and discussions

3.1. Meteorological data

An overview of the meteorological parameters during the measurements is given in Fig. 3. All data are 10 min averages. The temperature varied between 25.9 °C and 37.4 °C with an average of 31.2 °C. RH shows an anti-correlation with temperature at high levels of 80–100% during the night with an overall average of 77%. For the purpose of our further analysis, the meteorological data are classified into four types depending on the meteorological conditions. A brief illustration for the meteorological data recorded from 10 to 24 July is shown in Table 2. Type I and Type III conditions can be characterized as clear, sunny days with strong solar radiation and high wind speed. However, the dominant wind directions of Type I and Type III are different: North-West (from the mainland) and South-East (from the sea), respectively. For Type II, light wind and high solar radiation favors the accumulation of locally emitted pollutants on the measurement site, leading to high O_3 formation. The typhoon occurring during 15–18 July (Type IV) caused low solar radiation and temperature while the humidity was relatively high.

3.2. Time series of trace gases

Fig. 4 shows time series of the mixing ratios of SO_2, O_3, HCHO, NO_2 and HONO measured by the DOAS system and the corresponding ratios of $HONO/NO_2$ for the field measurements from 10 to 24 July. Evidently, under Type II meteorological conditions all trace gases tended to accumulate and reached high concentrations, whereas frequent rainfall accompanying the typhoon during the Type IV period removed pollutants by wet deposition, resulting in low concentration levels. During the whole measurement period SO_2 mixing ratios varied between 2.75 ± 0.1 and 320.78 ± 16.0 ppb. Peaks were usually observed at about 0000–0100 LT at midnight and around 0700–0900

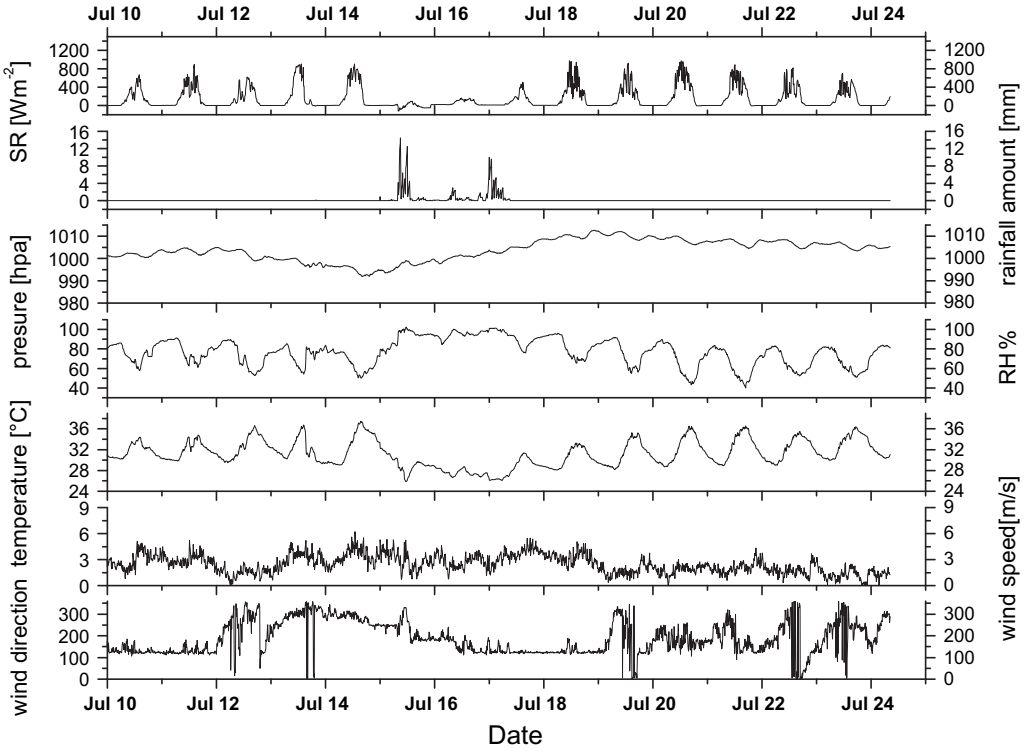

Fig. 3. Solar radiation (SR), 10-min integrated rainfall, pressure, relative humidity (RH), temperature, wind speed and wind direction for the whole measurement period.

Table 2
Classification of meteorological conditions during the field campaign 10–24 July, 2006.

Period	Classification	Wind direction	Avg. wind speed (m s^{-1})	Avg. temp. (°C)	Avg. RH (%)	Avg. SR (W m^{-2})	Remarks
10–11 July	Type I	NW	3	31.7	77.7	146.5	Clear sunny day
12 July 19–24 July	Type II	VRB (variable)	<2	32.2	69.9	172.9	Haze events
13–14 July	Type III	SE	3.2	32.4	70.6	195.7	Clear sunny day
15–18 July	Type IV	SW–SE	3.1	28.9	90.1	83.4	Typhoon period, rainfall

LT in the morning. The diurnal trend of SO_2 strongly depends on local residents' daily activities and for the time considered here was presumably strongly influenced by an increased demand of air conditioning, i.e. enhanced activity of power generators (Hu et al., 2002). As is typical of urban areas, O_3 shows a strong diurnal variation with low concentration at night and in the morning and peaks during the afternoon. Two O_3 pollution episodes appeared, one lasting several days from 19 to 24 July (O_3-maximum = 149.9 ± 7.6 ppb), another occurred on 12 July. The same trend in the distribution of HCHO and NO_2 was observed. During the whole measurement period, the HCHO took a mean of ~8.1 ppb with a maximum of 30.0 ± 1.6 ppb, whereas the mean and maximum of NO_2 were ~30.3 ppb and 116.7 ± 4.1 ppb, respectively. The measured HONO concentrations ranged from 0.71 ± 0.1 ppb to 8.43 ± 0.4 ppb, with a mean of ~2.8 ppb. Unexpected high HONO mixing ratios were observed even during the typhoon period. The HONO to NO_2 ratio exhibits a diurnal variation with low levels during daytime and high values during the second half of the night. Distinct peaks around midday could be observed on several days (e.g. 13, 14 and 20 July). The ratio ranged from 0.03 to 0.37 during the whole measurement period. Its maximum value (0.37 ± 0.09, occurred on 20 July) is much higher than that of previously reported values, varying between 0.01 and 0.1 (Alicke et al., 2002, 2003; Acker et al., 2006a). We compared these HONO data obtained by DOAS with those from the GAC instrument (see Section 2.2.2) and found general agreement ($r^2 = 0.62$) with a tendency of higher HONO concentrations for the GAC (Gu et al., 2009). Bearing in mind the complications of this measurement method remarked upon in the introduction, we do not pursue this fact any further here.

3.3. Correlation between HONO and NO_2 and possible sources of HONO

3.3.1. The diurnal variation of HONO, NO_2 and HONO/NO_2

The average diurnal variations of HONO, NO_2 as well as the ratios of HONO-to-NO_2, along with the solar radiation are shown in Fig. 5. To get representative diurnal variation, the data during the typhoon period were removed from the data set.

Since the measurement site was located in a region with heavy traffic, NO_2 concentrations remained at high levels even for large actinic fluxes. The lowest NO_2 mixing ratio of 18.7 ± 1.8 ppb was

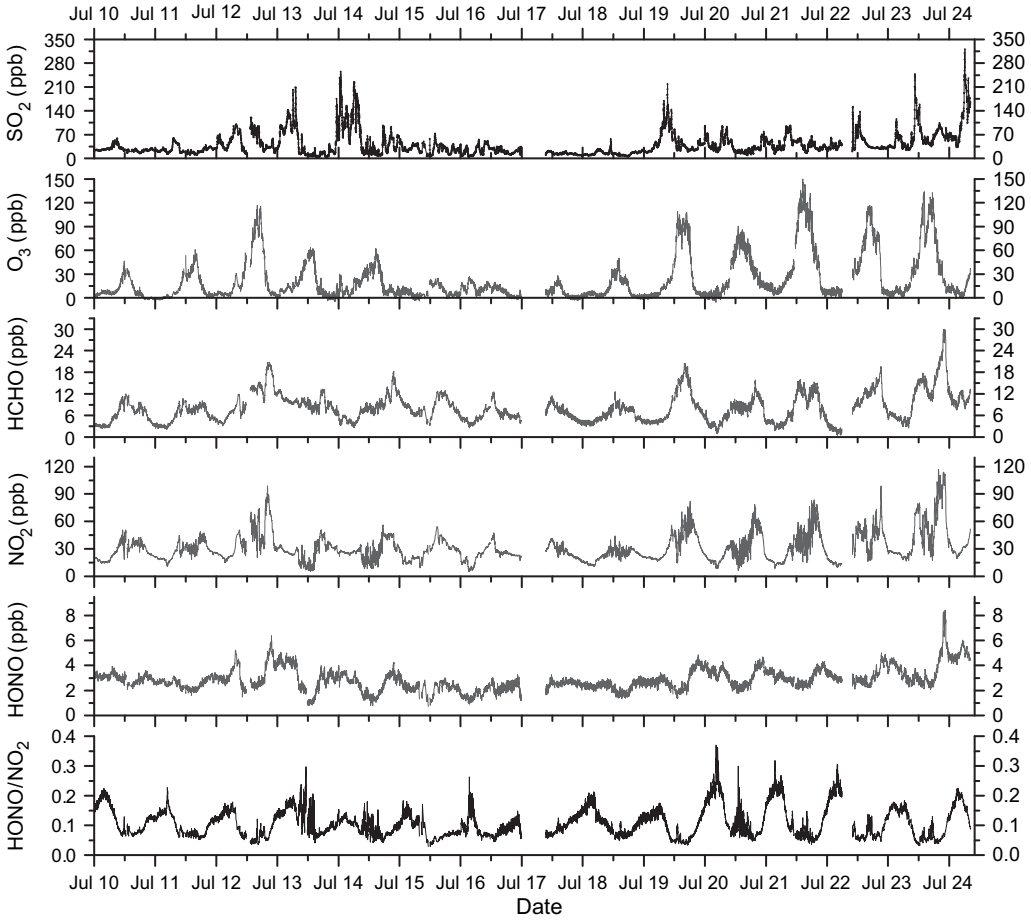

Fig. 4. Time series of trace gases measured by the DOAS system, 10–24 July.

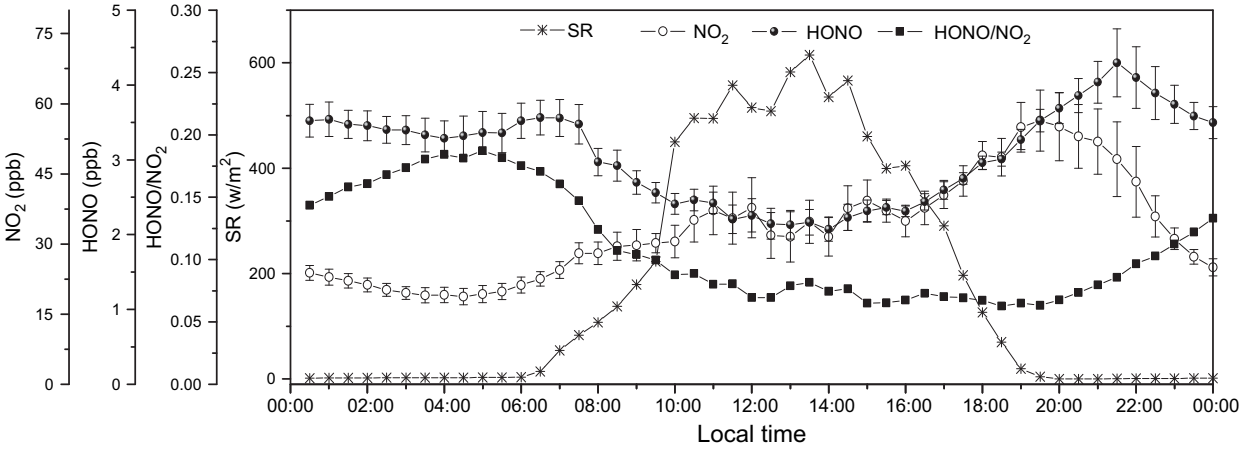

Fig. 5. Average diurnal patterns of HONO, NO_2 and the HONO-to-NO_2 ratio along with the solar radiation (the data obtained during the typhoon period was not included). The data are 30 min averages and the error bars for HONO and NO_2 represent the standard deviation within the measurement period.

observed at about 0430 LT and a nighttime maximum of 56.4 ± 6.5 ppb appeared at 1930 LT.

The diurnal pattern of HONO is similar to observations at other urban sites (Acker and Moller, 2007). Without photolysis HONO starts to increase right after sunset and accumulates during the night until an average maximum of ca. 4.3 ppb is reached around 2130 LT. Following, the HONO concentration remains at an almost constant value until a slight local maximum occurred during the morning rush hour. Finally, HONO decreases rapidly with the start of daytime photolysis and the destabilization of the nighttime boundary layer. The minimum value of 2 ppb is unexpected high, but consistent with results from the 2004 PRD campaign (Zhang et al., 2008) of up to 2 ppb. Our results for the daytime HONO mixing ratio are throughout considerably higher than recently reported values of about 130–300 ppt (Veitel et al., 2002; Acker et al., 2006a,b) of urban and rural sites in Europe.

The HONO-to-NO_2 ratio shows diurnal variations with low levels during daytime and high values during the second part of the night. Slight variations in the early afternoon might solely be due to changes of the solar radiation. An average nighttime conversion rate of about 0.016 h^{-1} for reaction (R6) was determined from the increase of the HONO-to-NO_2 ratio between 1930 and 2400 LT, which is in good agreement with other studies (Reisinger, 2000; Alicke et al., 2003; Kleffmann et al., 2003, 2005; Acker and Moller, 2007).

3.3.2. Direct emission of HONO

At the moment, emission inventories or emission factor databases of HONO are not available for the PRD region, which makes an estimate of any direct HONO emission very difficult. As there are no major point sources nearby the measurement site, we restrict ourselves to traffic induced emissions and consider only nighttime data (1800–0600 LT) to avoid problems related to the instant photolysis of directly emitted HONO. To get an upper limit of HONO emitted by traffic, we use emission ratios $[HONO]_{traffic}/[NO_x]_{traffic}$ obtained from tunnel measurements (Kurtenbach et al., 2001) and assume that all $NOx = NO_2 + NO$ measured by DOAS and commercial point monitors, respectively, is due to traffic. The maximum [NO]/$[NO_x]$ (representing air with fresh traffic emissions) for our nighttime values is about 0.89, agreeing with values of >0.9 observed by Kurtenbach et al. (2001), so that it might seem reasonable to adopt their emission ratio $[HONO]_{traffic}/[NO_x]_{traffic} = 0.65\%$. (Our minimum $[HONO]/[NO_x]$ value of 1.4% is somewhat higher than measured in the aforementioned study.) Based on the assumption that directly emitted HONO is not immediately transform, the HONO concentrations corrected by direct (traffic) emissions are therefore given by

$$[HONO]_{corr} = [HONO] - [HONO]_{em} = [HONO] - 0.0065 * [NO_x]$$

Fig. 6 shows the frequency distribution of nighttime $[HONO]_{em}/[HONO]$, where in total 1803 data points were included. It turns out that for this upper estimate about 80% of all ratios $[HONO]_{em}/[HONO]$ have values smaller than 15%, so that the direct emission of HONO is unlikely to be the reason of our observed nighttime HONO levels. Therefore, we only corrected the nighttime data used in the subsequent study of RH with HONO/NO_2.

3.3.3. Correlation between HONO and NO_2

NO_2 is known to be an important precursor for the formation of HONO or to have a common source. As mentioned in the introduction, the concentrations of HONO and NO_2 (or $NO \cdot NO_2$) were found to be highly correlated in many field observations. Acker et al. (2005) pointed out that different meteorological regimes can cause significant differences in the source receptor relation, resulting in very different types of correlation. They found that for low wind speeds the HONO concentrations were positively correlated with those of NO_2 ($r^2 = 0.72$) if all data (day and night) were used, while a separation of the data into sunlight and darkness hours did not

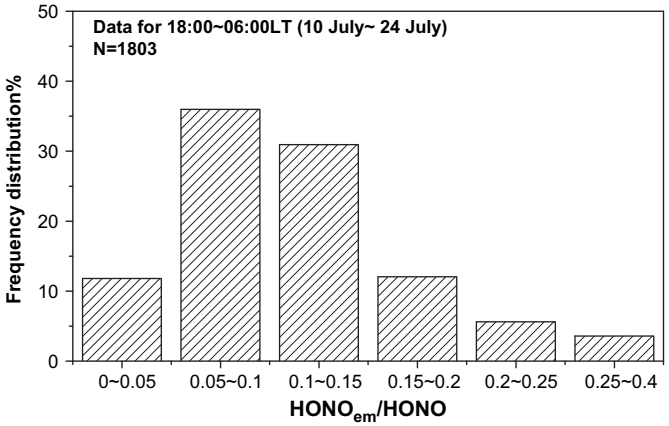

Fig. 6. Percentage distribution of the nighttime $[HONO]_{em}/[HONO]$ in 0.05 ratio intervals.

Table 3
Correlation studies between HONO and NO_2 for the Type II period.

Date	Time interval	Avg. wind speed (m s^{-1})	Number of data points	Correlation coefficient (r)	Slope	Intercept
12 July	1000–1700 LT	1.7	183	0.75	0.0169 ± 0.00131	1.58 ± 0.067
19 July	1000–1700 LT	1.4	252	0.75	0.0180 ± 0.00098	1.301 ± 0.041
20 July	1000–1700 LT	2.0	360	0.79	0.0219 ± 0.00107	1.74 ± 0.029
21 July	1100–1700 LT	2.1	247	0.81	0.0173 ± 0.00117	1.812 ± 0.044
22 July	1000–1700 LT	1.5	270	0.74	0.0168 ± 0.00103	2.003 ± 0.044
23 July	1100–1700 LT	1.6	182	0.72	0.0149 ± 0.00142	1.936 ± 0.079

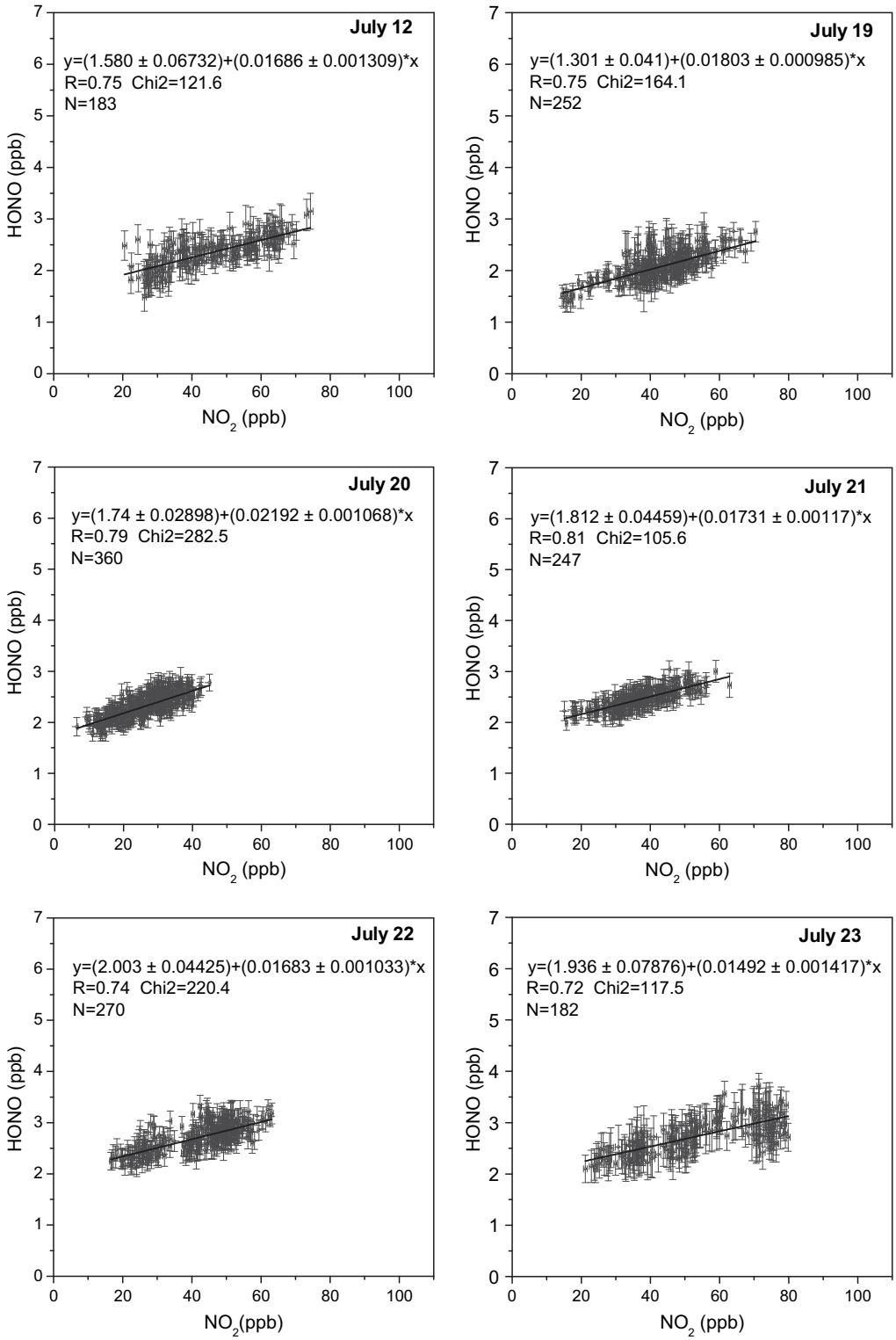

Fig. 7. Correlation between HONO and NO_2 between 1000 and 1700 LT during the Type II period.

improve the correlation. It should be mentioned that the early experiment by Harrison et al. (1996) in a central urban environment did not show a clear relationship between HONO and NO_2. However, studies carried out in China so far indicate a good correlation between the two species during the nighttime (Qin et al., 2006; Hao et al., 2006; Su et al., 2008a).

Here, we concentrate on the Type II period with low wind speed where the concentrations of the pollutants are high. For reasons mentioned in the previous section, the correlation with NO_2 is calculated for the total HONO, i.e. including possible direct emissions. Using both day and night data yields a correlation coefficient r less than 0.4 for this 6-day period, so that we divide the data set into sunlight and darkness hours for further interpretation. We found clear correlations for the daytime period of 1000–1700 LT (this time interval was considered to avoid complications from morning and evening rush hour traffic peaks). This is shown in Table 3, which lists details of our correlation studies. Fig. 7 contains correlation plots between HONO and NO_2 for each day individually.

A significant positive correlation $r > 0.7$ can be found for all days with fairly constant slopes varying between 0.015 and 0.022 at an average of 0.018 – a fact which might just reflect stable meteorology and emissions. Intercepts vary between 1.301 ± 0.041 and 2.003 ± 0.044. Similarly good correlations for the same daytime period emerge also for the 11, 13 and 14 July (not shown here). Unfortunately, data for OH and J(HONO) are not available for our measurements, so that a calculation of the photo-stationary state (PSS) concentration of HONO as in Kleffmann et al. (2005) is not possible. Physical processes (transport and diffusion) can also be an explanation of good correlation between pollutants. Using CO as a tracer for traffic induced emissions we tested this by considering the correlation between HONO and CO for the same time intervals. The much lower correlation coefficients between HONO and CO (r 0.07–0.67) indicate a minor effect of these processes for most of the cases. To examine the importance of the heterogeneous reaction (R8) as a daytime source of HONO, we next looked at the correlation between HONO and HNO_3 and aerosol nitrate, respectively, observed by the GAC for the same times intervals as in Table 3 (see Fig. 8). In agreement with a negligible photolysis of nitrate measured in chamber experiments (Rohrer et al., 2005), our data revealed a lower correlation between HONO and NO_3^- ($r = 0.5$) than between HONO and NO_2.

Turning to the nighttime, a good correlation between HONO and NO_2 could only be found for the second half of a few nights (e.g. 0000–0800 LT of 20–23 July), an observation similar to the one gained from the INTERCOMP2000 campaign in Melpitz (Acker et al., 2005). The general absence of correlation during the first half of the night can plausibly be explained by an increasing HONO-to-NO_2 ratio, if – after a stable nocturnal boundary layer has built up – HONO is produced via the heterogeneous pathway (R6) while NO_2 decreases, see also Harrison et al. (1996). When finally the production rate of HONO equals its loss (at night mainly deposition) a steady state is reached (Stutz et al., 2002). As suggested by Acker et al. (2005), hereafter the concentrations of HONO and NO_2 are dominated by physical and chemical processes other than straightforward NO_2–HONO reactions, which would result in a good correlation until the morning rush hour. Constant HONO mixing ratios in the second part of the night occurred indeed frequently during our campaign, see Figs. 4 and 5.

3.3.4. Aerosol impact on HONO formation

As mentioned in the introduction, it has been suggested that HONO can be created in heterogeneous reactions on ground or aerosol surfaces and several combined HONO and aerosol (surface area) observations indeed indicate that aerosols could be a major factor for HONO production (Notholt et al., 1992; Andres-Hernandez et al., 1996; Reisinger, 2000). Supporting this hypothesis, a close relationship between HONO/NO_2 and PM10 mass concentration ($r = 0.77$) was observed in an investigation of the effects of agricultural waste burning (Park et al., 2004). Other measurements, however, do not point into this direction: Gradient measurements (Kleffmann et al., 2003; Stutz et al., 2004b) found only a weak aerosol influence on HONO formation, in agreement with various laboratory studies on soot, aqueous/humid surfaces and organic particles (Kleffmann et al., 1998, 1999; Arens et al., 2001; Broske et al., 2003; Finlayson-Pitts et al., 2003). Up to now, the role aerosols play in the formation of HONO is still under discussion.

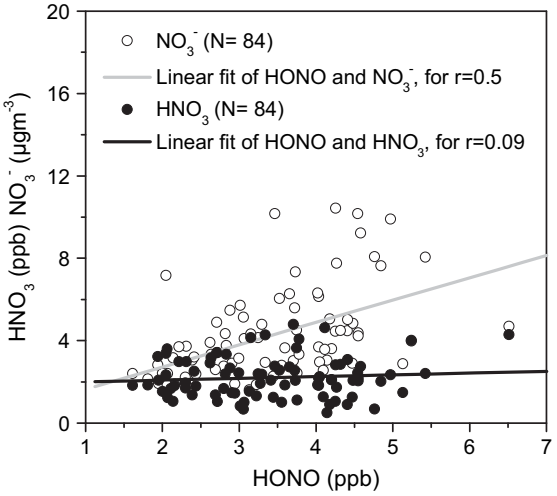

Fig. 8. Correlation study of HONO & HNO_3 and HONO & NO_3^- based on the GAC data obtained during the Type II period of 19–24 July. Time intervals are consistent with those listed in Table 3.

In this study, we mainly use the PM10 mass concentration to get an idea of the aerosol impact on the HONO production because the surface to volume ratio $S/V_{aerosol}$ is only available for the 5 days of 10 and 21–24 July. Fig. 9 shows the time series of HONO and HONO-to-NO_2 along with PM10, $S/V_{aerosol}$ and aerosol nitrite for the whole measurement period (all data averaged over 15 min). The two week average PM10 mass concentration was about 88 μg m^{-3} with a maximum of 278.9 μg m^{-3} occurring on the night of 23 July. The few available $S/V_{aerosol}$ data show a trend similar to PM10. While for some days (19–24 July) an obvious delay between the peaks of PM10 (or $S/V_{aerosol}$) and HONO exists, other days (13–15 July; first panel of Fig. 9, highlighted in grey) show coinciding trends of both concentrations. Fig. 10 reveals a strong linear correlation with $r = 0.81$ for these latter 3 days. This is interesting in that they are dominated by South-East wind from the sea and a consistent tendency for this period was also found in the time series of Cl^- (not shown here). During these days, a similar correlation occurs also between PM10 and the HONO-to-NO_2 ratio (especially for the 2 days of 13 and 14 July), see the grey shaded area in the second panel of Fig. 9. This fact is consistent with the supposition that sea-salt aerosol was involved in the conversion of NO_2 to HONO.

It was proposed that nitrite can be formed on humid surfaces or water droplets by the heterogeneous reactions (R6) (Lammel and Cape, 1996) and (R8) (Zhou et al., 2001). The surface adsorbed nitrite can be protonated into nitrous acid which is then released as gaseous HONO. In their field measurements of aerosol nitrite, Simon and Dasgupta (1995) observed a strong correlation with HONO in ambient air. For our measurements, such a relationship could not be identified.

We conclude here that a further discussion of the aerosol impact on HONO formation for our data requires more information on

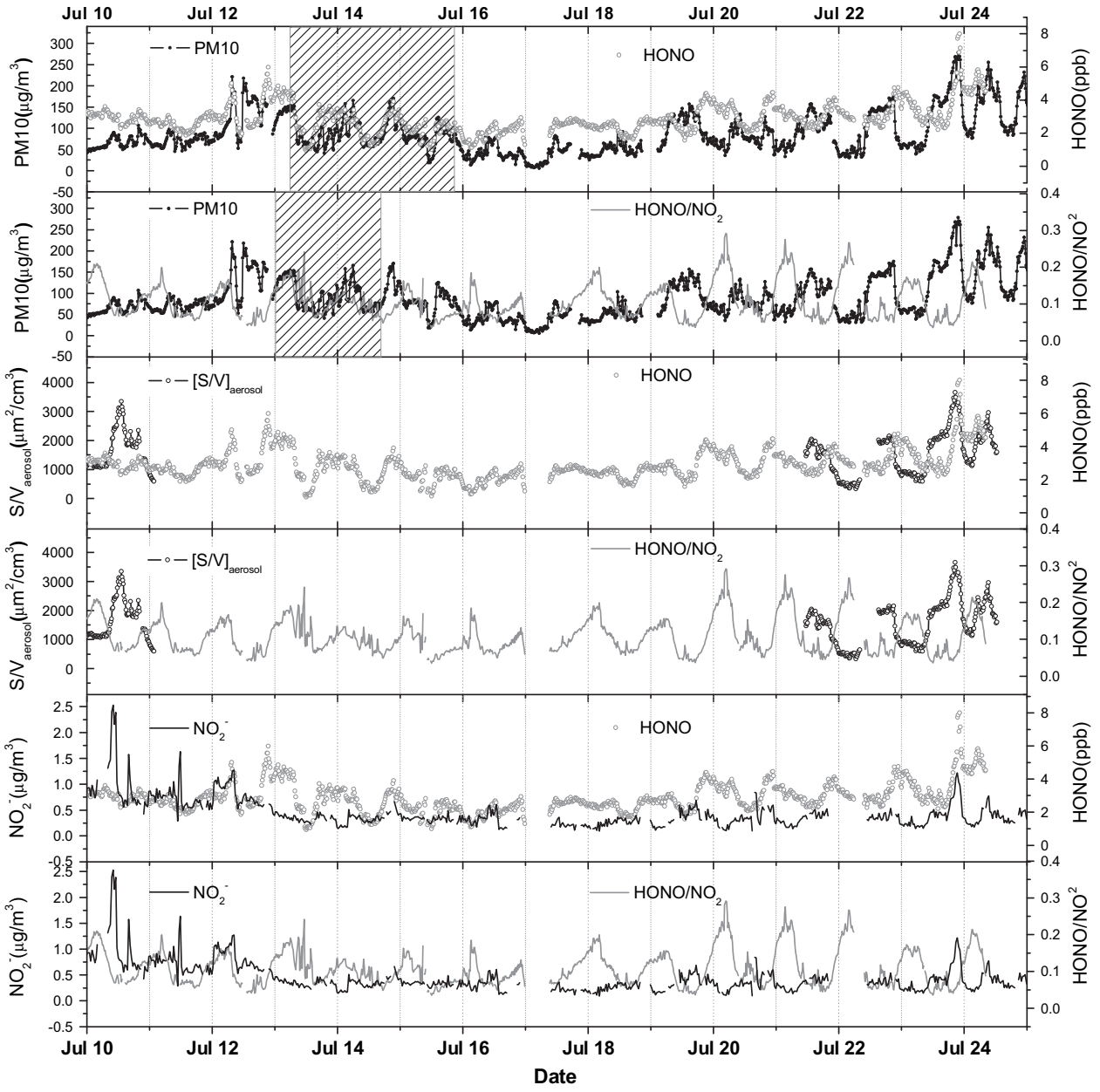

Fig. 9. Temporal variation of HONO (grey open circles) and HONO-to-NO_2 ratios (grey line) along with PM10 mass concentration (blank line with solid circles), $[S/V]_{aerosol}$ (black line with open circles) and aerosol nitrite (black line) during the study period. Dotted vertical lines indicate midnight (0000 LT). See text for the details.

source character and chemical composition of the aerosol distribution. In our case, building surfaces appear to play the main role for heterogeneous HONO formation.

3.3.5. *Relative humidity dependence of the HONO-to-NO_2 ratio*

Laboratory studies have demonstrated that water acts as an important component for nocturnal heterogeneous conversion of NO_2 to HONO (Jenkin et al., 1988; Svensson et al., 1987; Pitts et al., 1984). It appears that the amount of surface adsorbed water plays a more important role than the amount of water vapor (Finlayson-Pitts et al., 2003; Kleffmann et al., 1998), but the exact mechanisms are still unclear. Based on the data sets obtained in three field experiments at different locations in the United States, Stutz et al. (2004a) investigated the dependence of the net NO_2 to HONO conversion mechanism on the RH by using a pseudo steady state approach. The authors found that HONO/NO_2 ratios between 10% and 30% RH do not exceed 0.04, while values of up to 0.09 were observed at higher RH. A recent observation in China showed that the maximum HONO/NO_2 ratio increasing with RH below 70% and decreasing for RH > 70% (Hao et al., 2006). In the following, we closely follow the procedure by Stutz et al. (2004a) using the corrected HONO concentrations $[HONO]_{corr}$ from Section 3.3.2. To eliminate the interference caused by rainfall, the data acquired during rainy days are removed from the analysis. All nocturnal HONO-to-NO_2 ratios are averaged like the RH data over 10-min intervals. Fig. 11 sums up the statistical results including a total of 767 nighttime data, separated before and after midnight, with lowest measured RH values of about 45%. High $HONO_{corr}$-to-NO_2 ratios always occurred after midnight with high RH. As can be seen, $HONO_{corr}/NO_2$ ratios increase rapidly between 70% and 85% RH and drop again after RH reaches 85%. Between 45% and 70% RH average $HONO_{corr}/NO_2$ ratios vary slowly below a value of about 0.06.

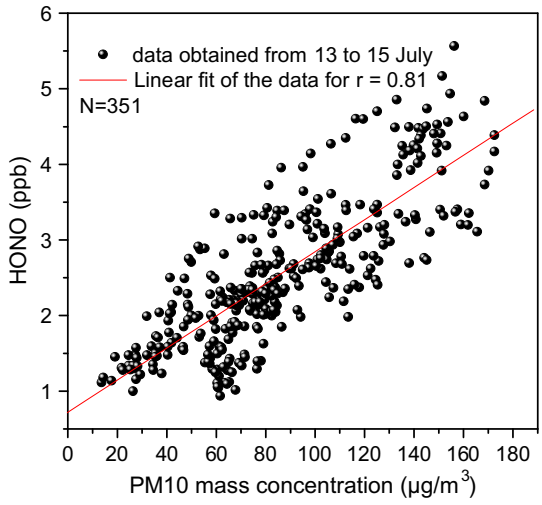

Fig. 10. Correlation study of HONO and PM10 for the period from 13 to 15 July.

Highest nighttime $HONO_{corr}/NO_2$ ratios close to 0.3 lay in the interval of 80–85% RH. A qualitative description of this behavior may be that the nocturnal boundary layer together with several high buildings providing the reaction surfaces for the heterogeneous reaction (R6) inhibit the exchange with fresh outside air, which – in combination with relatively high temperatures and RH – creates a "smog chamber"– like situation where NO_2 loss and nighttime production of HONO lead to high HONO-to-NO_2 ratios.

We followed the procedure described in (Stutz et al., 2004a) and calculated the averages of the five highest $HONO_{corr}/NO_2$ values (representing steady state conditions) in RH intervals of 5%. We then separately for both data sets performed a linear least squares fit to the corresponding RH averages and find distinct linear relationships between the "steady state" $[HONO]_{corr}/[NO_2]$ ratios and RH, as shown in Fig. 11, i.e. for our data a nocturnal heterogeneous conversion rate of NO_2 to HONO proportional to RH. We further notice a larger slope and therefore stronger dependence on RH for the second half of the night than for the first half. Secondly, we remark that the deviation from the linear relationship for the values before midnight in the RH interval between 70% and 75% can be traced back to the Type II period dominated by haze. While a dependency of the HONO formation on RH clearly exists for our data, the last two observations also show that its details are strongly coupled to the atmospheric conditions.

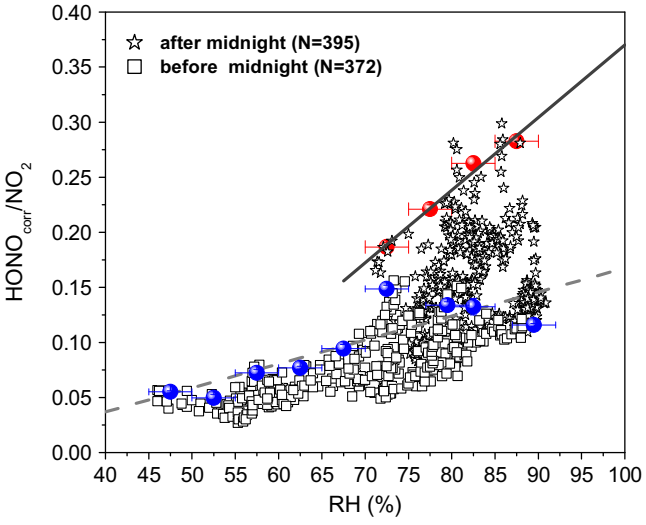

Fig. 11. Nighttime correlation study between $HONO_{corr}$-to-NO_2 ratios and RH, separating the data into "before midnight" (open squares) and "after midnight" (open start). Red and blue solid circles represent the averages of the five highest $HONO_{corr}/NO_2$ ratios in 5%-RH-intervals before and after midnight, respectively. The linear least squares fit through the two sets of corresponding RH averages is also shown in the figure (solid grey and dashed light grey line). See text for details. (For interpretation of the references to colour in this figure legend the reader is referred to the web version of this article.)

4. Conclusions

The trace gases HONO, NO_2, SO_2, O_3 and HCHO were measured at an urban site in Guangzhou city during the Pearl River Delta (PRD) 2006 intensive campaign by a differential optical absorption spectroscopy (DOAS) system. The variations of air pollutants were found to be closely related to the meteorological condition with high levels during two pollution episodes and low levels during a typhoon period from 15 to 18 July. Lowest average mixing ratios of NO_2 were observed at about 0430 LT and the average maximum appeared around 1730 LT. The diurnal pattern of HONO was similar to that observed at other urban sites. HONO concentrations varied between 0.71 ± 0.1 ppb and 8.43 ± 0.4 ppb during the whole measurement period, with a mean of about 2.8 ppb. The HONO-to-NO_2 ratios exhibited a distinct diurnal variation with low levels during daytime and high values during the second part of the night. The maximum ratio of 0.37 ± 0.09 was observed at the dawn of 20 July.

Various chemical and meteorological parameters were employed to discuss the correlation between HONO and NO_2 and the existence of possible HONO sources. On average, a strong positive correlation between HONO and NO_2 was found during 1000–1900 LT, in contrast to previous observations in China. Using a literature value of 0.0065 for the traffic induced emission ratio of $HONO/NO_x$, a minor impact of HONO direct traffic emission on the observed HONO data was found.

Combining the information of PM10, $S/V_{aerosol}$ and aerosol nitrite measurement data, we conclude that aerosol had a minor influence on HONO formation during our measurements, whereas nighttime heterogeneous NO_2 to HONO conversion processes seem mainly to occur on building surfaces, significantly depending on RH. The very high $HONO_{corr}/NO_2$ values during the night constitute the most striking result of our study and will be subject of future research.

Acknowledgements

This work was supported by the National Natural Science Foundation of China: 40675072 and the China National Basic Research and Development Program 2002CB410801 and 2002CB211605. The authors would like to thank Sun Yet-Sen University for providing meteorological data and researchers and students of Peking University for their help during the 2006 PRD campaign. The authors would also like to thank Dr. Andreas Hartl for his English revisions. Special thanks are also given to the two anonymous reviewers for their kind suggestions to improve the quality of this manuscript.

References

Acker, K., Febo, A., Trick, S., Perrino, C., Bruno, P., Wiesen, P., Moller, D., Wieprecht, W., Auel, R., Giusto, M., Geyer, A., Platt, U., Allegrini, I., 2006a. Nitrous acid in the urban area of Rome. Atmospheric Environment 40, 3123–3133.

Acker, K., Moller, D., 2007. Atmospheric variation of nitrous acid at different sites in Europe. Environmental Chemistry 4, 242–255.

Acker, K., Moller, D., Auel, R., Wieprecht, W., Kalass, D., 2005. Concentrations of nitrous acid, nitric acid, nitrite and nitrate in the gas and aerosol phase at a site in the emission zone during ESCOMPTE 2001 experiment. Atmospheric Research 74, 507–524.

Acker, K., Moller, D., Wieprecht, W., Meixner, F.X., Bohn, B., Gilge, S., Plass-Dulmer, C., Berresheim, H., 2006b. Strong daytime production of OH from HNO2 at a rural mountain site. Geophysical Research Letters 33, 4.

Acker, K., Spindler, G., Bruggemann, E., 2004. Nitrous and nitric acid measurements during the INTERCOMP2000 campaign in Melpitz. Atmospheric Environment 38, 6497–6505.

Alicke, B., Geyer, A., Hofzumahaus, A., Holland, F., Konrad, S., Patz, H.W., Schafer, J., Stutz, J., Volz-Thomas, A., Platt, U., 2003. OH formation by HONO photolysis during the BERLIOZ experiment. Journal of Geophysical Research-Atmospheres 108, 17.

Alicke, B., Platt, U., Stutz, J., 2002. Impact of nitrous acid photolysis on the total hydroxyl radical budget during the Limitation of Oxidant Production/Pianura Padana Produzione di Ozono study in Milan. Journal of Geophysical Research-Atmospheres 107, 18.

Ammann, M., Kalberer, M., Jost, D.T., Tobler, L., Rossler, E., Piguet, D., Gaggeler, H.W., Baltensperger, U., 1998. Heterogeneous production of nitrous acid on soot in polluted air masses. Nature 395, 157–160.

Andres-Hernandez, M.D., Notholt, J., Hjorth, J., Schrems, O., 1996. A DOAS study on the origin of nitrous acid at urban and non-urban sites. Atmospheric Environment 30, 175–180.

Arens, F., Gutzwiller, L., Baltensperger, U., Gaggeler, H.W., Ammann, M., 2001. Heterogeneous reaction of NO2 on diesel soot particles. Environmental Science & Technology 35, 2191–2199.

Bejan, I., Abd El Aal, Y., Barnes, I., Benter, T., Bohn, B., Wiesen, P., Kleffmann, J., 2006. The photolysis of ortho-nitrophenols: a new gas phase source of HONO. Physical Chemistry Chemical Physics 8, 2028–2035.

Bejan, I., Barnes, I., Olariu, R., Zhou, S.M., Wiesen, P., Benter, T., 2007. Investigations on the gas-phase photolysis and OH radical kinetics of methyl-2-nitrophenols. Physical Chemistry Chemical Physics 9, 5686–5692.

Broske, R., Kleffmann, J., Wiesen, P., 2003. Heterogeneous conversion of NO2 on secondary organic aerosol surfaces: a possible source of nitrous acid (HONO) in the atmosphere? Atmospheric Chemistry and Physics 3, 469–474.

Cheng, Y.F., Eichler, H., Wiedensohler, A., Heintzenberg, J., Zhang, Y.H., Hu, M., Herrmann, H., Zeng, L.M., Liu, S., Gnauk, T., Bruggemann, E., He, L.Y., 2006. Mixing state of elemental carbon and non-light-absorbing aerosol components derived from in situ particle optical properties at Xinken in Pearl River Delta of China. Journal of Geophysical Research-Atmospheres. 111, D20204.

Finlayson-Pitts, B.J., Wingen, L.M., Sumner, A.L., Syomin, D., Ramazan, K.A., 2003. The heterogeneous hydrolysis of NO2 in laboratory systems and in outdoor and indoor atmospheres: an integrated mechanism. Physical Chemistry Chemical Physics 5, 223–242.

Fisseha, R., Dommen, J., Gutzwiller, L., Weingartner, E., Gysel, M., Emmenegger, C., Kalberer, M., Baltensperger, U., 2006. Seasonal and diurnal characteristics of water soluble inorganic compounds in the gas and aerosol phase in the Zurich area. Atmospheric Chemistry and Physics 6, 1895–1904.

George, C., Strekowski, R.S., Kleffmann, J., Stemmler, K., Ammann, M., 2005. Photoenhanced uptake of gaseous NO2 on solid-organic compounds: a photochemical source of HONO? Faraday Discussions 130, 195–210.

Gu, J.W., Zhang, Y.H., Zeng, L.M., Wen, M.T., 2009. Evaluation of the performance of a gas and aerosol collector (GAC). Research of Environmental Sciences-China 22, 16–22.

Guangdong Statistical Yearbook, 2006. Bureau of Statistics of Guangdong Province. China Statistics Press, Beijing. ISBN:7-5037-4904-0/F.2251.

Gustafsson, R.J., Orlov, A., Griffiths, P.T., Cox, R.A., Lambert, R.M., 2006. Reduction of NO2 to nitrous acid on illuminated titanium dioxide aerosol surfaces: implications for photocatalysis and atmospheric chemistry. Chemical Communications, 3936–3938.

Gutzwiller, L., Arens, F., Baltensperger, U., Gaggeler, H.W., Ammann, M., 2002. Significance of semivolatile diesel exhaust organics for secondary HONO formation. Environmental Science & Technology 36, 677–682.

Hao, N., Zhou, B., Chen, D., Chen, L.M., 2006. Observations of nitrous acid and its relative humidity dependence in Shanghai. Journal of Environmental Sciences-China 18, 910–915.

Harrison, R.M., Peak, J.D., Collins, G.M., 1996. Tropospheric cycle of nitrous acid. Journal of Geophysical Research-Atmospheres 101, 14429–14439.

Hu, M., Zhou, F.M., Shao, K.S., Zhang, Y.H., Tang, X.Y., Slanina, J., 2002. Diurnal variations of aerosol chemical compositions and related gaseous pollutants in Beijing and Guangzhou. Journal of Environmental Science and Health Part A-Toxic/Hazardous Substances & Environmental Engineering 37, 479–488.

Jenkin, M.E., Cox, R.A., Williams, D.J., 1988. Laboratory studies of the kinetics of formation of nitrous-acid from the thermal-reaction of nitrogen-dioxide and water-vapor. Atmospheric Environment 22, 487–498.

Kirchstetter, T.W., Harley, R.A., Littlejohn, D., 1996. Measurement of nitrous acid in motor vehicle exhaust. Environmental Science & Technology 30, 2843–2849.

Kleffmann, J., 2007. Daytime sources of nitrous acid (HONO) in the atmospheric boundary layer. Chemphyschem 8, 1137–1144.

Kleffmann, J., Becker, K.H., Lackhoff, M., Wiesen, P., 1999. Heterogeneous conversion of NO2 on carbonaceous surfaces. Physical Chemistry Chemical Physics 1, 5443–5450.

Kleffmann, J., Becker, K.H., Wiesen, P., 1998. Heterogeneous NO2 conversion processes on acid surfaces: possible atmospheric implications. Atmospheric Environment 32, 2721–2729.

Kleffmann, J., Gavriloaiei, T., Hofzumahaus, A., Holland, F., Koppmann, R., Rupp, L., Schlosser, E., Siese, M., Wahner, A., 2005. Daytime formation of nitrous acid: a major source of OH radicals in a forest. Geophysical Research Letters 32, 4.

Kleffmann, J., Kurtenbach, R., Lorzer, J., Wiesen, P., Kalthoff, N., Vogel, B., Vogel, H., 2003. Measured and simulated vertical profiles of nitrous acid – Part I: field measurements. Atmospheric Environment 37, 2949–2955.

Kleffmann, J., Lorzer, J.C., Wiesen, P., Kern, C., Trick, S., Volkamer, R., Rodenas, M., Wirtz, K., 2006. Intercomparison of the DOAS and LOPAP techniques for the detection of nitrous acid (HONO). Atmospheric Environment 40, 3640–3652.

Kurtenbach, R., Becker, K.H., Gomes, J.A.G., Kleffmann, J., Lorzer, J.C., Spittler, M., Wiesen, P., Ackermann, R., Geyer, A., Platt, U., 2001. Investigations of emissions and heterogeneous formation of HONO in a road traffic tunnel. Atmospheric Environment 35, 3385–3394.

Lammel, G., Cape, J.N., 1996. Nitrous acid and nitrite in the atmosphere. Chemical Society Reviews 25, 361–369.

Li, S.P., Matthews, J., Sinha, A., 2008. Atmospheric hydroxyl radical production from electronically excited NO2 and H2O. Science 319, 1657–1660.

Meller, R., Moortgat, G.K., 2000. Temperature dependence of the absorption cross sections of formaldehyde between 223 and 323 K in the wavelength range 225–375 nm. Journal of Geophysical Research-Atmospheres 105, 7089–7101.

Nguyen, M.T., Sumathi, R., Sengupta, D., Peeters, J., 1998. Theoretical analysis of reactions related to the HNO2 energy surface: OH + NO and H + NO2. Chemical Physics 230, 1–11.

Notholt, J., Hjorth, J., Raes, F., 1992. Formation of HNO2 on aerosol surfaces during Foggy periods in the presence of NO and NO2. Atmospheric Environment Part A-General Topics 26, 211–217.

Pagsberg, P., Bjergbakke, E., Ratajczak, E., Sillesen, A., 1997. Kinetics of the gas phase reaction OH + NO(+M) → HONO(+M) and the determination of the UV absorption cross sections of HONO. Chemical Physics Letters 272, 383–390.

Park, S.S., Hong, S.B., Jung, Y.G., Lee, J.H., 2004. Measurements of PM10 aerosol and gas-phase nitrous acid during fall season in a semi-urban atmosphere. Atmospheric Environment 38, 293–304.

Pitts, J.N., Sanhueza, E., Atkinson, R., Carter, W.P.L., Winer, A.M., Harris, G.W., Plum, C.N., 1984. An investigation of the dark formation of nitrous-acid in environmental chambers. International Journal of Chemical Kinetics 16, 919–939.

Qin, M., Xie, P.H., Liu, W.Q., Li, A., Dou, K., Fang, W., Liu, H.G., Zhang, W.J., 2006. Observation of atmospheric nitrous acid with DOAS in Beijing, China. Journal of Environmental Sciences-China 18, 69–75.

Ramazan, K.A., Syomin, D., Finlayson-Pitts, B.J., 2004. The photochemical production of HONO during the heterogeneous hydrolysis of NO2. Physical Chemistry Chemical Physics 6, 3836–3843.

Reisinger, A.R., 2000. Observations of HNO_2 in the polluted winter atmosphere: possible heterogeneous production on aerosols. Atmospheric Environment 34, 3865–3874.

Rohrer, F., Bohn, B., Brauers, T., Bruning, D., Johnen, F.J., Wahner, A., Kleffmann, J., 2005. Characterisation of the photolytic HONO-source in the atmosphere simulation chamber SAPHIR. Atmospheric Chemistry and Physics 5, 2189–2201.

Simon, P.K., Dasgupta, P.K., 1995. Continuous automated measurement of gaseous nitrous and nitric-acids and particulate nitrite and nitrate. Environmental Science & Technology 29, 1534–1541.

Stemmler, K., Ammann, M., Donders, C., Kleffmann, J., George, C., 2006. Photosensitized reduction of nitrogen dioxide on humic acid as a source of nitrous acid. Nature 440, 195–198.

Stemmler, K., Ndour, M., Elshorbany, Y., Kleffmann, J., D'Anna, B., George, C., Bohn, B., Ammann, M., 2007. Light induced conversion of nitrogen dioxide into nitrous acid on submicron humic acid aerosol. Atmospheric Chemistry and Physics 7, 4237–4248.

Stuhl, F., Niki, H., 1972. Pulsed vacuum-UV photochemical study of reactions of OH with H2, D2, and Co using a resonance-fluorescent detection method. Journal of Chemical Physics 57, 3671–3677.

Stutz, J., Alicke, B., Ackermann, R., Geyer, A., Wang, S.H., White, A.B., Williams, E.J., Spicer, C.W., Fast, J.D., 2004a. Relative humidity dependence of HONO chemistry in urban areas. Journal of Geophysical Research-Atmospheres 109, 14.

Stutz, J., Alicke, B., Ackermann, R., Geyer, A., White, A., Williams, E., 2004b. Vertical profiles of NO3, N2O5, O-3, and NOx in the nocturnal boundary layer: 1. Observations during the Texas air quality study 2000. Journal of Geophysical Research-Atmospheres 109.

Stutz, J., Alicke, B., Neftel, A., 2002. Nitrous acid formation in the urban atmosphere: gradient measurements of NO2 and HONO over grass in Milan, Italy. Journal of Geophysical Research-Atmospheres 107, 16.

Stutz, J., Kim, E.S., Platt, U., Bruno, P., Perrino, C., Febo, A., 2000. UV–visible absorption cross sections of nitrous acid. Journal of Geophysical Research-Atmospheres 105, 14585–14592.

Stutz, J., Platt, U., 1996. Numerical analysis and estimation of the statistical error of differential optical absorption spectroscopy measurements with least-squares methods. Applied Optics 35, 6041–6053.

Su, H., Cheng, Y.F., Cheng, P., Zhang, Y.H., Dong, S.F., Zeng, L.M., Wang, X.S., Slanina, J., Shao, M., Wiedensohler, A., 2008a. Observation of nighttime nitrous acid (HONO) formation at a non-urban site during PRIDE-PRD2004 in China. Atmospheric Environment 42, 6219–6232.

Su, H., Cheng, Y.F., Shao, M., Gao, D.F., Yu, Z.Y., Zeng, L.M., Slanina, J., Zhang, Y.H., Wiedensohler, A., 2008b. Nitrous acid (HONO) and its daytime sources at a rural site during the 2004 PRIDE-PRD experiment in China. Journal of Geophysical Research-Atmospheres 113.

Svensson, R., Ljungstrom, E., Lindqvist, O., 1987. Kinetics of the reaction between nitrogen-dioxide and water-vapor. Atmospheric Environment 21, 1529–1539.

Vandaele, A.C., Simon, P.C., Guilmot, J.M., Carleer, M., Colin, R., 1994. SO2 Absorption cross-section measurement in the UV using a Fourier-transform spectrometer. Journal of Geophysical Research-Atmospheres 99, 25599–25605.

Veitel, H., Kromer, B., Mossner, M., Platt, U., 2002. New techniques for measurements of atmospheric vertical trace gas profiles using DOAS. Environmental Science and Pollution Research, 17–26.

Voigt, S., Orphal, J., Bogumil, K., Burrows, J.P., 2001. The temperature dependence (203–293 K) of the absorption cross sections of O-3 in the 230–850 nm region measured by Fourier-transform spectroscopy. Journal of Photochemistry and Photobiology A-Chemistry 143, 1–9.

Voigt, S., Orphal, J., Burrows, J.P., 2002. The temperature and pressure dependence of the absorption cross-sections of NO2 in the 250–800 nm region measured by Fourier-transform spectroscopy. Journal of Photochemistry and Photobiology A-Chemistry 149, 1–7.

Zhang, Y.H., Su, H., Zhong, L.J., Cheng, Y.F., Zeng, L.M., Wang, X.S., Xiang, Y.R., Wang, J.L., Gao, D.F., Shao, M., Fan, S.J., Liu, S.C., 2008. Regional ozone pollution and observation-based approach for analyzing ozone-precursor relationship during the PRIDE-PRD2004 campaign. Atmospheric Environment 42, 6203–6218.

Zhou, X.L., Beine, H.J., Honrath, R.E., Fuentes, J.D., Simpson, W., Shepson, P.B., Bottenheim, J.W., 2001. Snowpack photochemical production of HONO: a major source of OH in the Arctic boundary layer in springtime. Geophysical Research Letters 28, 4087–4090.

Zhou, X.L., Gao, H.L., He, Y., Huang, G., Bertman, S.B., Civerolo, K., Schwab, J., 2003. Nitric acid photolysis on surfaces in low-NOx environments: significant atmospheric implications. Geophysical Research Letters 30, 4.

Zhou, X.L., He, Y., Huang, G., Thornberry, T.D., Carroll, M.A., Bertman, S.B., 2002. Photochemical production of nitrous acid on glass sample manifold surface. Geophysical Research Letters 29 (14), 1681.